Effects of Convective Transport on Chemical Signal Propagation in Epithelia

Marek Nebyla, Michal Přibyl,* and Igor Schreiber
Department of Chemical Engineering, Institute of Chemical Technology, Prague, Czech Republic

ABSTRACT We study effects of convective transport on a chemical front wave representing a signal propagation at a simple (single layer) epithelium by means of mathematical modeling. Plug flow and laminar flow regimes were considered. We observed a nonmonotonous dependence of the propagation velocity on the ligand receptor binding constant under influence of the convective transport. If the signal propagates downstream, the region of high velocities becomes much broader and spreads over several orders of magnitude of the binding constant. When the convective transport is oriented against the propagating signal, either velocity of the traveling front wave is slowed down or the traveling front wave can stop or reverse the direction of propagation. More importantly, chemical signal in epithelial systems influenced by the convective transport can propagate almost independently of the ligand-receptor binding constant in a broad range of this parameter. Furthermore, we found that the effects of the convective transport becomes more significant in systems where either the characteristic dimension of the extracellular space is larger/comparable with the spatial extent of the ligand diffusion trafficking or the ligand-receptor binding/ligand diffusion rate ratio is high.

INTRODUCTION

Short-distance (autocrine or paracrine) signaling in epithelia is mediated by extracellular signaling molecules that bind to membrane receptors. Growth factors (signaling molecules) and protein tyrosin kinase receptors constitute an important class of the ligand-receptor pairs in signal transmission. Proper combination of the growth factor stimuli at the receptors determines the cell fate, e.g., proliferation, apoptosis, differentiation, resting, etc. (1). Growth factor signaling is also responsible for complex processes such as wound healing (2) or organ development (3).

It was usually considered that growth factors are transported only by diffusion in the extracellular matrix. However, recent findings revealed that the convective transport can also significantly contribute to the total transport. Some developmental processes are even impossible when convection is suppressed (4). For example, an oriented convective transport induced by cilia at the ventral node of embryos is responsible for formation of the left-right body axis (5,6). Pressure gradients that emerge in a body during muscle contractions or body movement result in interstitial flow that can be observed almost in all tissues (4,7). In some of them vascular system is absent therefore the interstitial flow is necessary for nutrient supply. Interestingly, oscillatory pressure gradients imposed on osteoblast cells induce their proliferation (8).

Interstitial flow is able to promote migration of several cell types when endothelial tissue is damaged. The convective flow then plays an important role in vascular injury healing (9,10). Generally, the interstitial flow is important during angiogenesis or lymphangiogenesis. For example, lymphatic cells move, tend to be organized, and form new capillaries in the direction of the interstitial flow (11,12). Blood endothelial cells also develop vascular structures under influence of the convective flow (12,13). Number and length of new capillary structures depend on the mean velocity of the interstitial flow. In vitro experiments (14) showed that such dependence can be nonmonotonous with a maximum at 10–20 μm min^{-1}. During these developmental processes, the convective flow always works in synergy with signaling protein molecules such as vascular endothelial growth factor (VEGF) (12) or epidermal growth factor (EGF) (13).

Convection can play a specific role in tumor tissues. It is known that tumors are usually more permeable than healthy tissues and thus the pressure gradients can result in plasma extravasation (15). Signaling molecules produced by cancer cells or the cells themselves can easily migrate into surrounding tissue. Shear forces together with formed gradients of growth factors then lead to further vascular spouting (16). Such a process is called the autologous chemotaxis (17). On the other hand, the changes in permeability open new possibilities for cancer treatment (7,18).

Theoretical studies focused on the convective transport effects in various tissue systems have been reported. Chen et al. (19) studied velocity pattern, cilia rotation, and lateral displacement of cilia in embryonic ventral nodes during the left-right axis body formation. Nguyen et al. (20) modeled vascular system formation in a yolk sac. They considered effects such as the Poiseuille flow or tissue deformation. Helm et al. (12) and Fleury et al. (21) showed that oriented convective transport forms specifically localized gradients of VEGF or other morphogens, which leads to cell chemotaxis and vascular system formation in the direction of the flow. Their model is based on the local mass balance

Submitted November 22, 2011, and accepted for publication January 23, 2012.

*Correspondence: pribylm@vscht.cz

Editor: Stanislav Shvartsman.

0006-3495/12/03/0990/11 $2.00

doi: 10.1016/j.bpj.2012.01.038

of a morphogen and the Brinkman equation for the velocity field evaluation around a cell. Relevant to our topic are also a number of studies on reaction-diffusion-convection waves and patterns contributed from the chemical engineering community, particularly those primarily related to spatially two-dimensional (2D) modeling (22–24).

In this work, we deal with effects of the convective flow on velocity of signal transmission mediated by protein growth factors (particularly by EGFs) and tyrosin kinase transmembrane receptors at epithelial tissues. We assume that ligand trafficking occurs in a narrow gap between a cellular layer and a semipermeable membrane. Such epithelia are formed from mammal astrocytes (18), mammal enterocytes (25), *Drosophila melanogaster* follicle cells (26), etc. Growth factor signaling is then responsible for glioblastoma multiforme appearance in mammals or dorsal appendage formation in *Drosophila* oocytes.

For this study, we adopted a mathematical model reported in (27). The model describes the growth factor signal propagation above an epithelium as a result of reaction-transport positive feedback called the ligand-induced ligand release. We extend the model by introducing the convective transport. More specifically, plug and laminar flows are considered above the epithelium layer. We found an exact solution of the mathematical model in an asymptotic regime. The full model was analyzed numerically. We particularly focus on the effect of the Péclet number on the propagation velocity. The Péclet number, being the ratio of fluxes due to convection and diffusion, is a quantitative measure of the convective transport intensity. Even for the Péclet number less than one, the convective transport qualitatively alters the morphogen fields at epithelium and thus significantly affects developmental and other tissue processes (4,21).

MATHEMATICAL MODEL

Qualitative aspects

Reaction and transport processes considered in our model are summarized in Fig. 1. The epithelial cells are exposed to an extracellular environment where the transport of signal molecules occurs. We assume that a ligand (growth factor) is transported by diffusion and convective transport mechanisms. A semipermeable membrane, e.g., the blood-brain barrier that separates circulating blood and the extracellular fluid in the brain tissue, limits the ligand trafficking to a narrow gap above the epithelium. The ligand can reversibly form complexes with the growth factor receptor found on the cytoplasmic membrane of glial or other epithelium cells. Formation of the ligand-receptor complexes leads to triggering of an intracellular phosphorylation cascade and follow-up processes. Above a certain (threshold) level of the complex concentration, an intracellular or surface protease initiates a release of new ligand molecules into extracellular space. These processes form a positive feedback loop that enables signal propagation above the epithelial tissue. The ligand-receptor complex and the receptor itself are internalized and then destroyed by endocytosis. Here, we assume that the rate of formation of new receptors is constant and the ligand is not significantly degraded by extracellular proteases (28). The positive feedback present in the system generates bistability, which in turn implies the occurrence of traveling front waves.

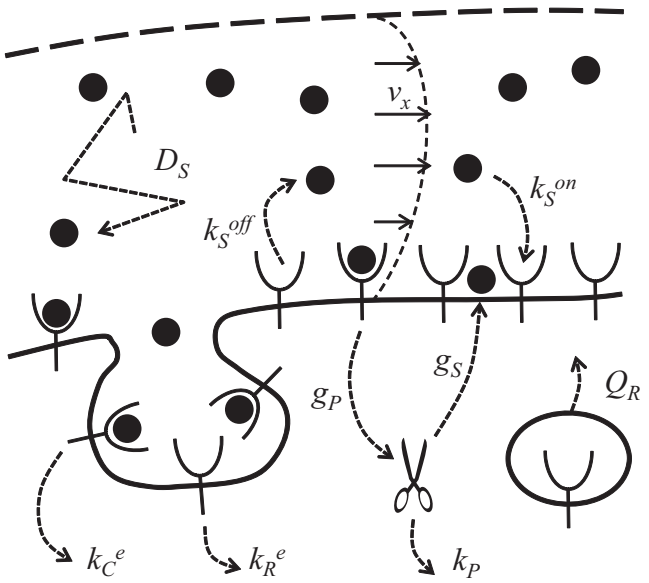

FIGURE 1 Reaction transport processes at the epithelium. The parameter meaning is summarized in Table 1.

To study velocity of signal transmission mediated by the extracellular ligand, we considered a simplified 2D domain shown in Fig. 2. All the transport processes occur in an extracellular gap of thickness H. The epithelium and semipermeable membrane represent the bottom and top boundaries of the modeling domain, respectively.

Furthermore, we consider the plug flow or Poiseuille flow in the extracellular gap. There are many experimental works dealing with in vitro cellular systems—three-dimensional cellular matrixes (12–14,29–31) or 2D cellular layers (25,32–35) and with effects of convection on cellular system development. The plug flow model can be applied to three-dimensional porous structures with certain dispersion

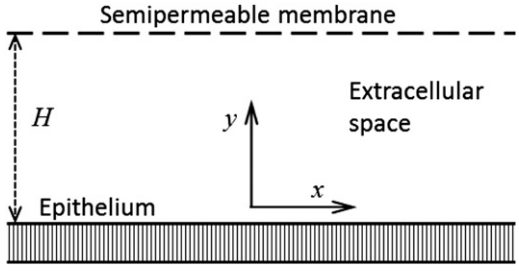

FIGURE 2 Geometry of the modeling domain.

limitations. The laminar flow model is applicable to another class of biological systems: flat cellular cultures on dishes, transforming follicular epithelia that are in contact with an oocyte via an extracellular gap, thin vein capillaries, etc. In addition, the laminar flow assumption is relevant to geometrically well-defined microfluidic experiments with in vitro cell cultures (32–35).

Model equations

Distribution of the ligand molecules in the gap is described by the mass balance

$$\frac{\partial S}{\partial t} + v_x(y)\frac{\partial S}{\partial x} = D_S\left(\frac{\partial^2 S}{\partial x^2} + \frac{\partial^2 S}{\partial y^2}\right), \quad (1)$$

where S denotes the ligand concentration and D_S is the ligand diffusivity. Spatially isotropic diffusion transport is considered. We assume that the convective flow of the extracellular medium is directed along the epithelium layer (x direction). The momentum equations are not considered. Instead, the flow regime in the gap is approximated by either the plug flow, Eq. 2, or laminar (parabolic) flow, Eq. 3 (36–38),

$$v_x(y) = v_x^{av}, \quad (2)$$

$$v_x(y) = \frac{6v_x^{av}(Hy - y^2)}{H^2}, \quad (3)$$

where v_x^{av} is the mean velocity in the x direction.

At the cellular boundary ($y = 0$), the ligands together with the receptors R can reversibly form the ligand-receptor complex C. New ligand molecules are released at this boundary by the protease P

$$-D_S\frac{\partial S}{\partial y} = -k_S^{on}SR + k_S^{off}C + g_S P,\ y = 0. \quad (4)$$

The symbols k_S^{on}, k_S^{off}, and g_S denote the ligand-receptor binding constant, the ligand-receptor dissociation constant, and the amplitude of the ligand release, respectively. The top boundary ($y = H$) is assumed impermeable for the ligand

$$-D_S\frac{\partial S}{\partial y} = 0,\ y = H. \quad (5)$$

The receptor dynamics is given by

$$\frac{\partial R}{\partial t} = Q_R - k_S^{on}SR + k_S^{off}C - k_R^e R, \quad (6)$$

where Q_R and k_R^e are the rate of the receptor formation and the receptor internalization constant, respectively.

The dynamics of ligand-receptor complex formation as well as the complex internalization process are expressed as

$$\frac{\partial C}{\partial t} = k_S^{on}SR - k_S^{off}C - k_C^e C. \quad (7)$$

The symbol k_C^e represents the internalization rate constant.

Activity of the ligand releasing protease is nonlinearly dependent on the ligand-receptor concentration

$$\frac{\partial P}{\partial t} = g_P\tilde{\sigma}(C) - k_P P, \quad (8)$$

where g_P and k_P are the protease amplification constant and the protease degradation rate constant, respectively. Signal output (e.g., protease activity) of an intracellular phosphorylation cascades (MAPK) can be described as a sigmoidal function $\tilde{\sigma}$ of the input to the cascade (e.g., the ligand-receptor complex concentration) (39,40). The sigmoidal function represents the sensitivity of the protease activation relative to a certain threshold concentration C_T of the ligand-receptor complex. The sigmoidal function works as a switch of the autocrine loop. We approximate the sigmoidal dependence by means of the following normalized function

$$\tilde{\sigma}(C) = 0.5\tanh\left[\frac{(C - C_T)}{\delta}\right] + 0.5, \quad (9)$$

where δ is a parameter affecting steepness of the sigmoidal function. The right-hand side of Eq. 9 provides effectively the same dependence on the complex concentration as the Hill cooperative kinetics of a high order. The Hill coefficient corresponding to the response of the MAPK cascade to the ligand stimulus is on the order of tens (41). We do not consider any time delay between the ligand-receptor binding and the protease activation. This effect has been studied in (27) and generally leads to a decrease of the propagation velocity.

Typical values of the model parameters were adopted from works (7,27,42) and are summarized in Table 1.

TABLE 1 Model parameters

Parameter	Range
C_T complex concentration threshold	$0<C_T<C_0$
D_S ligand diffusivity	$1\times10^{-12} - 1\times10^{-10}$ m^{2}s^{-1}
g_P amplification constant	
g_S intensity of ligand release	
$g_S g_P$	$1\times10^{-17} - 1\times10^{-15}$ mol m^{-2}s^{-2}
H gap thickness	$1\times10^{-7} - 1\times10^{-4}$ m
k_C^e internalization constant	$1.67\times10^{-3} - 5\times10^{-3}$ s^{-1}
k_P protease degradation constant	$1.67\times10^{-4} - 5\times10^{-4}$ s^{-1}
k_R^e internalization constant	$1.67\times10^{-4} - 1.67\times10^{-3}$ s^{-1}
k_S^{off} ligand dissociation constant	$1.67\times10^{-6} - 0.167$ s^{-1}
k_S^{on} ligand binding constant	$16.7 - 1.67\times10^{4}$ m^{3}mol^{-1}s^{-1}
Q_R receptor formation rate	$1\times10^{-14} - 1\times10^{-12}$ mol m^{-2}s^{-1}
v_x^{av} mean velocity	$-10 - 10\times10^{-6}$ m s^{-1}

Dimensionless model

Equations 1–8 were transformed into a dimensionless form to reduce the number of free model parameters. The scaling factor for the receptor concentration is chosen equal to the maximal possible concentration R_0. The protease concentration is scaled with the value of protease activity P_0 that is established at the equilibrium if the autocrine loop is switched on ($\tilde{\sigma} = 1$). The ligand-receptor and ligand concentrations are scaled with the corresponding binding/dissociation equilibrium concentrations C_0 and S_0 when the protease and receptor concentrations are considered equal to P_0 and R_0, respectively. The reciprocal protease degradation time constant was chosen as the timescale. The spatial coordinates x and y are scaled with the characteristic ligand diffusion length above the cell surface x_0 (43) and the extracellular gap thickness y_0, respectively. The velocity scale v_{x0} is equal to the characteristic velocity of the ligand diffusion. The list of the scaling constants is as follows:

$$\begin{aligned} S_0 &= \frac{C_0 k_R^e \left(k_S^{off} + k_C^e\right)}{k_S^{on} Q_R}, \quad R_0 = \frac{Q_R}{k_R^e}, \\ C_0 &= \frac{g_P g_S}{k_P k_C^e}, \qquad\qquad P_0 = \frac{g_P}{k_P}, \\ t_0 &= \frac{1}{k_P}, \quad x_0 = \frac{k_R^e D_S}{Q_R k_S^{on}}, \quad y_0 = H, \quad v_{x0} = \frac{D_S}{x_0}. \end{aligned} \tag{10}$$

In the dimensionless representation, the ligand local balance takes the following form,

$$\tau_S \frac{\partial \tilde{S}}{\partial \tilde{t}} + \tilde{v}_x\left(\tilde{y}\right)\frac{\partial \tilde{S}}{\partial \tilde{x}} = \frac{\partial^2 \tilde{S}}{\partial \tilde{x}^2} + \frac{1}{\alpha^2}\frac{\partial^2 \tilde{S}}{\partial \tilde{y}^2}, \tag{11}$$

where τ_S denotes the relative ligand timescale. We note that the parameter α can be interpreted in two ways, either as the Damköhler number, i.e., the ratio of the characteristic rates of ligand-receptor binding and ligand diffusion, or as the ratio of the two geometric scaling factors, i.e., y_0/x_0 (Table 2).

TABLE 2 Dimensionless parameters, basic set of parameters

Parameter	Basic value
$\alpha = HQ_R k_S^{on}/(k_R^e D_S) = y_0/x_0$	Varied
$\beta_S = k_C^e/(k_S^{off} + k_C^e)$	0.5
$\gamma = g_P g_S (k_S^{off} + k_C^e)/(k_P Q_R k_C^e)$	1
$\tilde{\delta} = \delta/C_0$	0.01
$\tau_C = k_P/(k_S^{off} + k_C^e)$	0.1
$\tau_R = k_P/k_R^e$	0.5
$\tau_S = k_R^{e2} D_S k_P/(Q_R k_S^{on})^2$	0.002
$\tilde{C}_T = C_T/C_0$	0.3
$Pe = v_x^{av} x_0/D_S$	Varied

The dimensionless velocities for the plug flow and laminar flow, respectively, are

$$\tilde{v}_x\left(\tilde{y}\right) = \mathrm{Pe}, \tag{12}$$

$$\tilde{v}_x\left(\tilde{y}\right) = 6\mathrm{Pe}\left(\tilde{y} - \tilde{y}^2\right), \tag{13}$$

where Pe is the Péclet number.

The corresponding dimensionless boundary conditions are

$$-\frac{\partial \tilde{S}}{\partial \tilde{y}} = \alpha\left[(1-\beta_S)\tilde{C} - \tilde{S}\tilde{R} + \beta_S \tilde{P}\right], \ \tilde{y} = 0 \tag{14}$$

$$\frac{\partial \tilde{S}}{\partial \tilde{y}} = 0, \ \tilde{y} = 1, \tag{15}$$

where β_S expresses the relative rate of the ligand-receptor complex endocytosis. We assumed that the ligand concentrations at $\tilde{x} \to \pm\infty$ attain the values corresponding to two spatially uniform stable steady states identified in the model equations. One of them corresponds to epithelium, which is not affected by the ligand ($\tilde{\sigma} = 0$). The steady state of the system is then: $\tilde{C} = 0$, $\tilde{P} = 0$, $\tilde{R} = 1$, $\tilde{S} = 0$. The other steady state corresponds to the protease activation switched on ($\tilde{\sigma} = 1$): $\tilde{C} = 1$, $\tilde{P} = 1$, $\tilde{R} = 1 - \gamma\beta_S$, $\tilde{S} = 1/(1 - \gamma\beta_S)$.

Equations 6 and 7 for the receptor and ligand-receptor complex are transformed into the dimensionless form

$$\tau_R \frac{\partial \tilde{R}}{\partial \tilde{t}} = 1 + \gamma\left[-\tilde{S}\tilde{R} + (1-\beta_S)\tilde{C}\right] - \tilde{R}, \tag{16}$$

$$\tau_C \frac{\partial \tilde{C}}{\partial \tilde{t}} = \tilde{S}\tilde{R} - \tilde{C}, \tag{17}$$

where γ is proportional to the ligand/receptor generation rate ratio. The symbols τ_R and τ_C denote the relative timescales of the kinetic processes.

Finally, the protease equation takes a simple form

$$\frac{\partial \tilde{P}}{\partial \tilde{t}} = \tilde{\sigma}\left(\tilde{C} - \tilde{C}_T\right) - \tilde{P}, \tag{18}$$

$$\tilde{\sigma}\left(\tilde{C} - \tilde{C}_T\right) = 0.5 \tanh\left[\frac{\left(\tilde{C} - \tilde{C}_T\right)}{\tilde{\delta}}\right] + 0.5. \tag{19}$$

Definitions of all dimensionless parameters of the model are summarized in Table 2 together with the basic set of their values. Equations 11–19 were solved numerically. However, for an asymptotic regime with the plug flow transport, we found an exact solution, see Appendix. This asymptotic solution can be used for the estimation of the

chemical signal propagation velocity for physically realistic parameter values but not within the entire range of the model parameters.

Traveling wave one-dimensional (1D) model

The dimensionless 2D model with the plug flow velocity profile (Eq. 12) introduced in the previous section can be reduced to a 1D model. If we assume that $y_0 \ll x_0$, i.e., $\alpha \ll 1$, the system becomes effectively 1D with only x as the spatial variable and the spatially averaged ligand concentration in the y direction,

$$\widehat{\tilde{S}}\left(\tilde{x}\right) \equiv \int_0^1 \tilde{S}\left(\tilde{x},\tilde{y}\right) d\tilde{y}, \tag{20}$$

will become a new variable of the 1D model (36,37). We note that the spatial averaging is generally not applicable for the laminar flow profile systems, Eq. 13. Because the ligand signaling is expected to take the form of a traveling front wave, we further transform the model into a traveling waveform amenable to a continuation analysis. Hence, we define a new moving coordinate ξ

$$\xi \equiv \tilde{x} - \tilde{u}\tilde{t}, \tag{21}$$

where $\tilde{u}$ is the dimensionless velocity of the chemical signal propagating as a front wave above the epithelial layer.

With the use of the thin fin approximation, Eq. 20, and the moving coordinate, Eq. 21, the model equations take the form

$$\frac{d^2\widehat{\tilde{S}}}{d\xi^2} + \left(\tau_S\tilde{u} - \mathrm{Pe}\right)\frac{d\widehat{\tilde{S}}}{d\xi} + \frac{1}{\alpha}\left[(1-\beta_S)\tilde{C} - \widehat{\tilde{S}}\tilde{R} + \beta_S\tilde{P}\right] = 0, \tag{22}$$

$$-\tilde{u}\tau_R\frac{d\tilde{R}}{d\xi} = 1 + \gamma\left[-\widehat{\tilde{S}}\tilde{R} + (1-\beta_S)\tilde{C}\right] - \tilde{R}, \tag{23}$$

$$-\tilde{u}\tau_C\frac{d\tilde{C}}{d\xi} = \widehat{\tilde{S}}\tilde{R} - \tilde{C}, \tag{24}$$

$$-\tilde{u}\frac{d\tilde{P}}{d\xi} = \tilde{\sigma}\left(\tilde{C} - \tilde{C}_T\right) - \tilde{P}, \tag{25}$$

with boundary conditions

$$\begin{aligned} &\tilde{x}\to+\infty, \quad \tilde{C}=0, \ \tilde{P}=0, \quad \tilde{R}=1, \quad \tilde{S}=0,\\ &\tilde{x}\to-\infty, \quad \tilde{C}=1, \ \tilde{P}=1, \quad \tilde{R}=1-\gamma\beta_S,\\ &\qquad\qquad \tilde{S}=1/(1-\gamma\beta_S). \end{aligned} \tag{26}$$

Numerical analysis

Dynamic simulations and continuations

To study behavior of the cellular system in broad ranges of the model parameters, we used several numerical solvers. Dynamical simulations were carried out using the Comsol Multiphysics 3.5 software package. The spatially 2D model domain was discretized using triangular finite elements. The element count depends on the size of the computation domain. The maximum element size used at the cellular boundary was $\Delta\tilde{x} = 0.05$. An increment of the same size was also used for solving the 1D problem when the approximation $\alpha \ll 1$ was applied. The dynamical femtime procedure used a standard odepack linear solver. The absolute and relative tolerances of the dynamical solver were set to 1×10^{-6} for all dimensionless variables.

We also used the continuation software package AUTO (44) for parametric analysis of the traveling wave 1D model. Front waves correspond to heteroclinic trajectories connecting two steady states. Continuation of the heteroclinics yields the velocity of front wave propagation in dependence on a control parameter.

Model validation

We first validated our 2D Comsol codes by means of the asymptotic 2D solution ($\gamma\to0$, $\tau_C\to0$), see Appendix. The solid line in Fig. 3 shows that the numerical codes

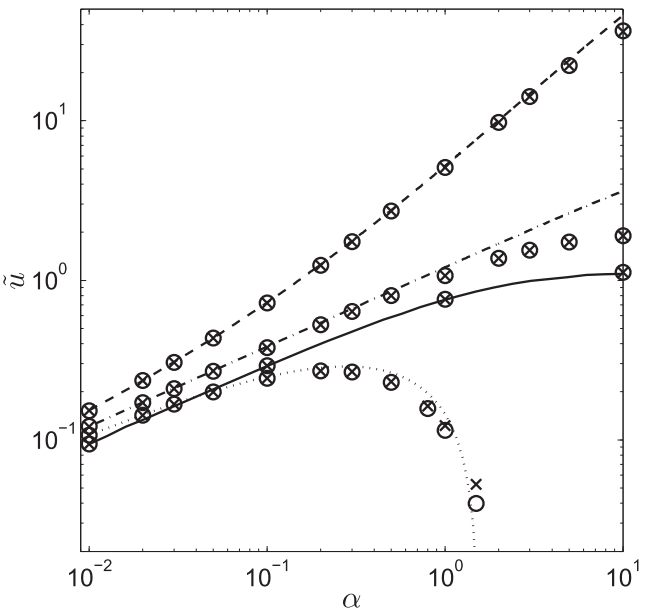

FIGURE 3 Dependence of the front wave propagation velocity on the Damköhler number. Solid line, 2D asymptotic solution (Pe = 0, $\gamma\to0$, $\tau_C\to0$); dashed line, continuation of the 1D traveling wave model (Pe = 1, $\gamma = 1$, $\tau_C = 0.1$); dash-dotted line, continuation of the 1D traveling wave model (Pe = 0, $\gamma = 1$, $\tau_C = 0.1$); dotted line, continuation of the 1D traveling wave model (Pe = −0.5, $\gamma = 1$, $\tau_C = 0.1$). Other parameters are listed in Table 2. Circles and crosses denote results of the Comsol dynamical simulations for the 2D-plug flow and the 2D-laminar flow models, respectively.

predict consistent behavior with the exact solution in a wide range of the Damköhler number α.

Outside the asymptotic regime, we compared predictions of the continuation analysis of the 1D model with the results of our 2D Comsol codes. We conclude that the 1D model provides results comparable with those of the more realistic 2D models up to $\alpha \approx 1$. This finding is consistent with the geometric interpretation of the parameter α expressing the scale ratio y_0/x_0. The thin fin approximation, Eq. 20, is certainly not justified for $\alpha>1$.

Furthermore, we observed that both of the 2D models involving the plug and laminar flow provide nearly the same propagation velocities. Significant differences were found only for $\mathrm{Pe} = -0.5$ and $\alpha>1$. In this case, the convective flow is oriented against the direction of the wave propagation but the wave velocity is very slow. The laminar flow is characterized by zero velocity at the cellular surface, i.e., the convective transport does not affect the ligand molecule transport. Due to the constant velocity profile of the plug flow, the ligand transport in such a case is decelerated via convection at the cellular surface.

The reason why the 2D plug and 2D laminar flow models usually give almost identical results as shown in Fig. 3 can be explained by the method originally introduced by Aris (45) for description of the Taylor dispersion in tubular systems. By applying this method, Kolev and van der Linden (46) derived a formula for evaluation of the dispersion coefficient D_T for fully developed parallel plate laminar flow. When neglecting the time decaying terms, the formula can be written for our system in the form

$$D_T = D_L\left(1 + \alpha^2 \mathrm{Pe}^2/210\right). \tag{27}$$

In Fig. 3, the highest values of the Damköhler and Péclet numbers are $\alpha = 10$ and $\mathrm{Pe} = 1$. Thus, the contribution of the ligand diffusivity to the overall dispersivity is always higher than the contribution due to the parabolic velocity profile.

We conclude that the simple 2D plug flow model is mostly a fair approximation applicable in a wide range of the model parameter values. Moreover, the simplified 1D model is usable with negligible errors up to $\alpha \approx 1$.

RESULTS AND DISCUSSION

Effects of convection - asymptotic analysis

Intuitively, positive Péclet number (the convective flow is oriented in the direction of the x axis) accelerates the signal propagation in the entire range of the Damköhler number, Fig. 3. Convective transport oriented against the direction of the x axis ($\mathrm{Pe}<0$) can stop the signal transmission originally oriented in the positive x direction.

One of the main results reported in (27) was that there is a robust maximum in the dependence of the propagation velocity on the forward binding rate constant. The nonmonotonous dependence results from the fact that low ligand-receptor affinity cannot give rise to the complex formation. On the other hand, extremely high affinity suppresses ligand random walks above the cellular layer. Let us assume that all assumptions for the use of the exact traveling wave plug-flow model (Appendix) are satisfied. It is of interest to then exactly evaluate common effects of the convective transport and binding constant on the velocity of signal propagation, Fig. 4.

Convection has only a weak effect for low values of $k_S^{on}R_0$. Such regimes correspond to low values of the parameter α, i.e., $H \ll x_0$. The characteristic velocity of the diffusion transport then becomes D_S/H rather than D_S/x_0. The Péclet number is then $\mathrm{Pe} = v_x^{av}H/D_S \ll 1$, which means that the effect of convection is negligible.

Convection becomes important for higher values of the binding constant. Fig. 4 clearly shows that a negative Péclet number decelerates the signal propagation velocity, which can stop the signal propagation. Significant acceleration of the velocity is manifested for $\mathrm{Pe}>1$. When the binding constant is high, convective transport is dominant and helps the ligand molecules to reach free receptors at a large distance from the front head. If compared to the system without convection ($\mathrm{Pe} = 0$), the propagation velocity is increased by two orders of magnitude, which occurs for example at $\mathrm{Pe} = 4$, $k_S^{on}R_0 = 10\ \mu\mathrm{m\ s}^{-1}$.

In the system without the convective transport, the highest propagation velocity occurs at $k_S^{on}R_0 = 0.01\ \mu\mathrm{m\ s}^{-1}$. If the

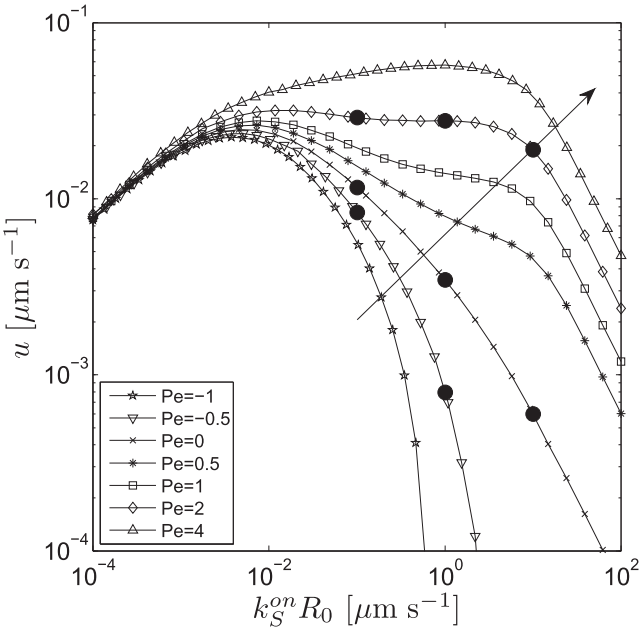

FIGURE 4 Dependence of the dimensional velocity of the signal propagation on the forward ligand-receptor binding rate, $h = 0.975 \times 10^{-5}\mathrm{m}$, $D = 1.61 \times 10^{-11}\mathrm{m^2 s^{-1}}, k_p = 3.4 \times 10^{-4}\mathrm{s^{-1}}, \beta_S = 0.5, \tilde{C}_T = 0.3,\ \gamma \to 0$, $\tau_C \to 0$. The large dots represent regimes for which the front waves are plotted in Fig. 5.

convective flow of a relatively low intensity ($\mathrm{Pe} \geq 1$) is oriented in the direction of the signal propagation, there is a region with high velocity spreading over three orders of magnitude ($k_S^{on} R_0 \in [0.01; 10]\ \mu\mathrm{m\ s}^{-1}$). This finding suggests that in epithelial systems properly influenced by convective transport, chemical signal can propagate almost independently of the ligand-receptor binding constant. Such effect can be exploited for example in tissue engineering (29,47). However, we have not found any systematic experimental study focused on the binding constant effects under the influence of the interstitial flow.

We can conclude that, at least in the studied range of the Péclet number, the nonmonotonous dependence of the signal propagation and the existence of the velocity maximum remain robust properties of the studied system. Furthermore, convective transport of a relatively low intensity can accelerate or decelerate the velocity of signal propagation by several orders of magnitude. Such a strong effect even for a low Péclet number was also reported by Fleury et al. (21), who studied a cellular system with a secreted protease releasing an extracellular matrix bound morphogen (VEGF).

In the next step, the character of the propagating ligand front waves was examined. When $k_S^{on} R_0 = 0.1\ \mu\mathrm{m\ s}^{-1}$, the form of the front wave is effectively 1D, localized at the threshold value ($\tilde{C}_T = 0.3$), and almost independent of the Péclet number, Fig. 5, *A–C*. This regime corresponds to $\alpha \approx 0.06 \ll 1$, where the thin fin approximation is applicable, Eq. 20. If the ligand-receptor binding strength is higher ($k_S^{on} R_0 = 1\ \mu\mathrm{m\ s}^{-1}$, $\alpha \approx 0.6$), the front wave still dominantly develops in the horizontal direction; however, it becomes elongated especially for $\mathrm{Pe} = 2$, Fig. 5, *D–F*. In this regime, convective transport dominates over diffusion and the ligand molecules are pushed away from the place of their release. For $k_S^{on} R_0 = 10\ \mu\mathrm{m\ s}^{-1}$ ($\alpha \approx 6$), shapes of the ligand front waves are spatially 2D, Fig. 5, *G* and *H*. The crucial effect of the convective transport on the front wave elongation can be seen in Fig. 5, *F–H*. Similar deformations of the morphogen concentration fields have been described in reports (12,21).

Effect of convection - general behavior

The exact solution used in the previous section was derived for positive propagation velocity ($\tilde{u} > 0$) in an asymptotic case, see Appendix. Here, we present results of a continuation analysis of the simplified 1D model. The basic set of parameter values (Table 2), for which the continuations were carried out, was approximately calculated from geometric means of the parameter ranges considered in Table 1.

Dependences of the propagation velocity on the Péclet number for three values of the Damköhler number are plotted in Fig. 6. We used the inverse hyperbolic sinus function (asinh) to visualize both the positive and negative values of the velocity in a logarithmic-like scale. Fig. 6 reveals two important facts. The convective transport significantly affects only such epithelium systems, in which characteristic dimension of the extracellular space is larger or comparable to the mean spatial extent of the ligand diffusion trafficking x_0. When $\alpha \ll 1$, i.e., $H \ll x_0$, the convective transport can be neglected as discussed in the previous section.

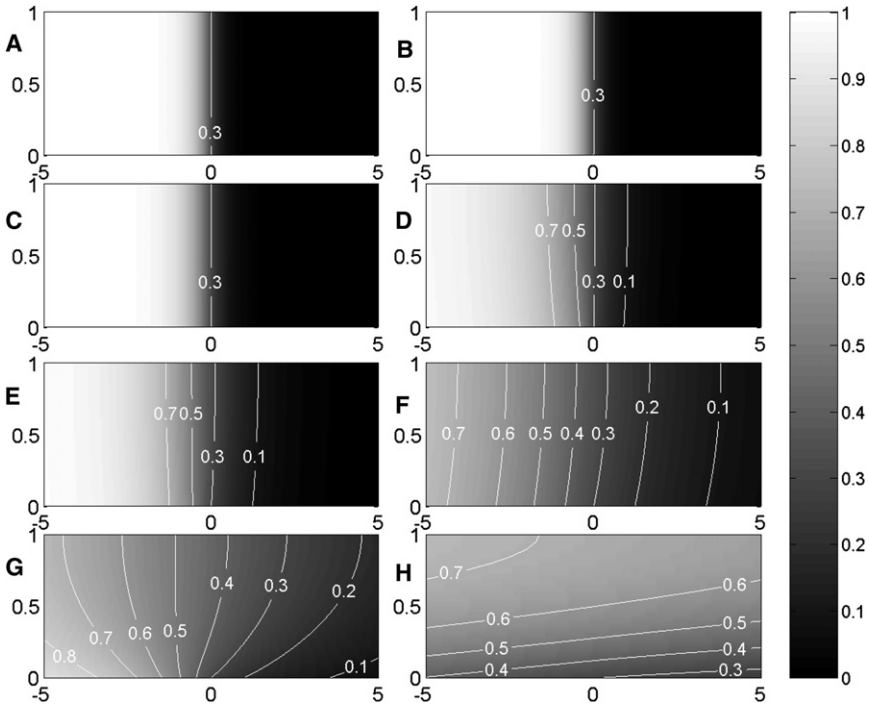

FIGURE 5 Propagating front waves of the autocrine communication. Values of the dimensionless ligand concentration $\tilde{S}$ are plotted in the spatial domain $\xi \in [-5, 5] \times \tilde{y} \in [0, 1]$. The ligand fields correspond to the large dots in Fig. 4. (*A*) $k_S^{on} R_0 = 0.1\ \mu\mathrm{m\ s}^{-1}$, $\mathrm{Pe} = -0.5$; (*B*) $k_S^{on} R_0 = 0.1\ \mu\mathrm{m\ s}^{-1}$, $\mathrm{Pe} = 0$; (*C*) $k_S^{on} R_0 = 0.1\ \mu\mathrm{m\ s}^{-1}$, $\mathrm{Pe} = +2$; (*D*) $k_S^{on} R_0 = 1\ \mu\mathrm{m\ s}^{-1}$, $\mathrm{Pe} = -0.5$; (*E*) $k_S^{on} R_0 = 1\ \mu\mathrm{m\ s}^{-1}$, $\mathrm{Pe} = 0$; (*F*) $k_S^{on} R_0 = 1\ \mu\mathrm{m\ s}^{-1}$, $\mathrm{Pe} = +2$; (*G*) $k_S^{on} R_0 = 10\ \mu\mathrm{m\ s}^{-1}$, $\mathrm{Pe} = 0$; and (*H*) $k_S^{on} R_0 = 10\ \mu\mathrm{m\ s}^{-1}$, $\mathrm{Pe} = +2$.

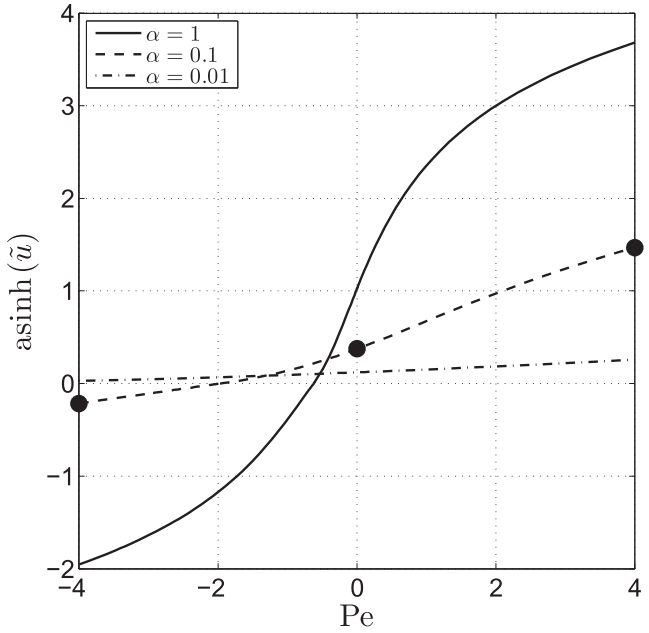

FIGURE 6 Dependence of the dimensionless velocity of the signal propagation on the Péclet number. Parameter values are given in Table 2. The black dots represent regimes plotted in Fig. 7.

If the convective flow becomes oriented against the original direction of the signal propagation (Pe < 0), the signal can be slowed, stopped, or reversed. Even if sensitivity of an epithelium layer to the ligand molecules is high, i.e., the threshold parameter $\tilde{C}_T$ is low, the system can switch from the protease active state ($\tilde{P} = 1$) to the inactive state ($\tilde{P} = 0$). Hence, properly oriented convective transport above epithelium can stop or probably eliminate various processes connected to the autocrine/paracrine chemical signal transmission, e.g., wound healing, tissue development, or cell proliferation. This finding is in agreement with available experimental data that show angiogenesis or lymphangiogenesis as processes occurring in the direction of the convective transport (12–14). Morphogen releasing molecules (proteases) or morphogens like VEGF or EGF, which control cell proliferation and/or cell motion, are released uniformly into the extracellular space if the convective flow is absent. Convection then breaks the spatial uniformity of the morphogen gradients and allows for oriented signal propagation.

The solid line in Fig. 7 represents a typical character of the propagating chemical wave switching the system from the protease active state to the inactive state ($\tilde{u}$>0) without any influence on the convective transport. The front wave is focused at the place of the threshold complex concentration value. Gradual decrease of the ligand and complex concentrations as well as the protease activity toward the protease inactive state is observed. The concentration of the free receptors increases accordingly.

Qualitative character of the front wave for Pe $= +4$ (*dash-dotted line* in Fig. 7) is similar because the propagation velocity is again positive. The front wave shape qualitatively changes when the direction of the signal propagation is reversed ($\tilde{u}$<0), the dashed line in Fig. 7. We can

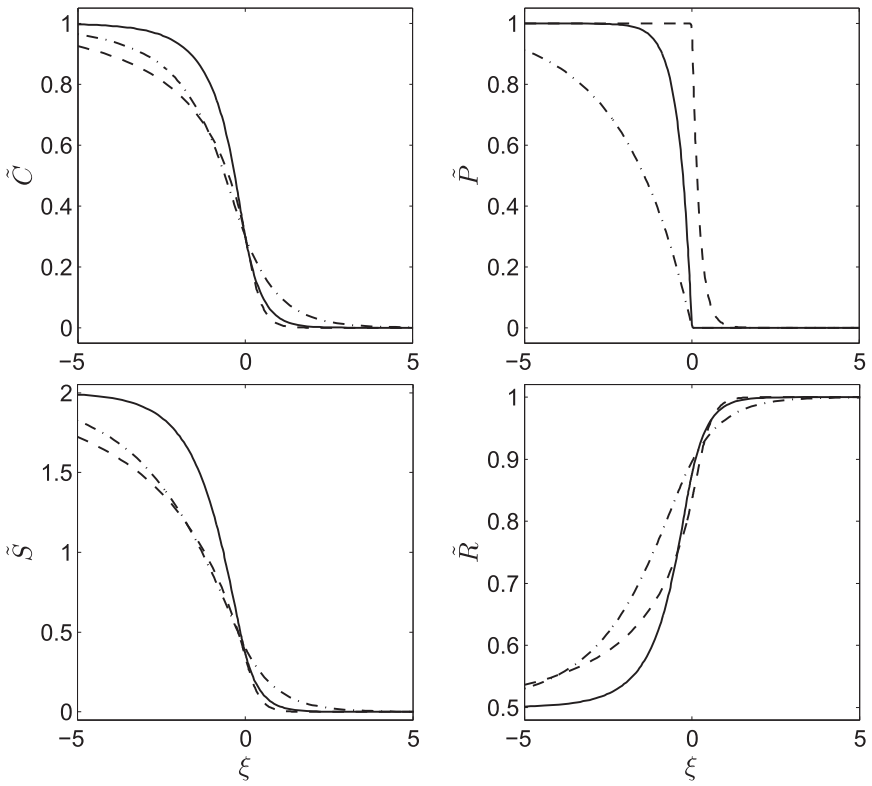

FIGURE 7 Propagating front waves of autocrine communication. Dashed line, Pe $= -4$, $\tilde{u} = -0.2164$; solid line, Pe $= 0$, $\tilde{u} = 0.3836$; dash-dotted line, Pe $= +4$, $\tilde{u} = 2.055$; $\alpha = 0.1$; the other parameters are given in Table 2.

observe a steep decrease of the protease activity at the place of the complex threshold concentration ($\tilde{C}_T$) as the front wave moves in the negative direction.

Substantial front wave elongation is observed in the presence of the convection (either positive or negative) due to the influenced ligand transport in the extracellular space, which is in agreement with data published in works (12,21).

CONCLUSIONS

The convective transport of morphogens significantly contributes to developmental and signaling processes in tissue systems. The presented theoretical study suggests that this is also valid in a simple epithelial system where the signal transmission is mediated by protein growth factors interacting with tyrosine kinase transmembrane receptors.

Our findings can be summarized as follows. The effects of the convective transport are important only if the characteristic dimension of the extracellular space is comparable or larger than the characteristic spatial extent of the ligand trafficking above the epithelium. The convective transport can then accelerate, stop, or even reverse the paracrine communication. If convection is oriented in the same direction as the original reaction-diffusion front wave, the propagation velocity of the chemical signaling becomes quite insensitive to the ligand-receptor binding constant. We also observe that the dependence of the propagation velocity on the binding constant remains nonmonotonous with a single maximum (27). The convective flow provides an elongation of the traveling front waves. Similar phenomenon was reported in other tissue systems affected by convection (12,21).

We have not found any experimental study focused exactly on velocity of the autocrine/paracrine signaling under the influence of convection. However, the reported studies confirm our findings indirectly. The oriented convective flow in model cellular tissues apparently accelerates and directionally favors developmental processes or cell movement. Because the developmental processes and cell chemotaxis are driven by morphogen or chemoattractant gradients, the convective transport must be responsible for acceleration or polarization of the signal transmission. For example, Park et. al. (34) found that mobility of mouse fibroblast cells increases with increasing shear stress (chemoattractant transport). Shin et. al. (35) reported that transfection efficiency in neuron cultures is also enhanced by shear stress (transport of exogeneous DNA molecules). Hernández Vera et. al. (14) showed that growing intensity of the interstitial flow can result in a significant length increase of formed endothelial capillary-like structures (morphogen transport).

We believe that these results can be useful in applications such as tissue engineering under controlled convective transport (47,48) or convention-enhanced delivery of chemotherapeutics (18). In the future, we will study effects of the oscillatory convective transport (49) and the convection-enhanced delivery of tyrosin kinase inhibitors (18,50) on the signal transmission velocity in epithelial tissues.

APPENDIX: TRAVELING WAVE PLUG FLOW MODEL—ASYMPTOTIC SOLUTION

An exact solution of the model Eqs. 11–12 and 14–19 can be obtained in a similar manner as in (27). We can assume a pseudosteady state for the ligand-receptor complex kinetics ($\tau_C \to 0$) if the extracellular transport and protease activation processes occur on larger timescales. The receptors are in a high surplus if a ligand-limited regime is considered, i.e. $\tilde{R} \approx 1$ may be a good approximation. Finally, the nonlinear protease activation term can be approximated by the Heaviside function ($\tilde{\sigma} \approx \tilde{H}$). This approximation is satisfied only if the intracellular processes lead to a sharp sigmoidal response, which is equivalent to a high value of the Hill coefficient of the cooperative enzyme kinetics (41).

We look for a solution in the form of a traveling front wave. The previous simplifications and the use of the transformation Eq. 21 result in simplified model equations

$$-\tilde{u}\frac{\partial \tilde{P}}{\partial \xi} + \tilde{P} = \tilde{H}\left(\tilde{S} - \tilde{C}_T\right), \tag{28}$$

$$\frac{\partial^2 \tilde{S}}{\partial \xi^2} + \left(\tau_S \tilde{u} - \mathrm{Pe}\right)\frac{\partial \tilde{S}}{\partial \xi} + \frac{1}{\alpha^2}\frac{\partial^2 \tilde{S}}{\partial y^2} = 0, \tag{29}$$

$$-\frac{\partial \tilde{S}}{\partial \tilde{y}} = \alpha\beta_S\left(\tilde{P} - \tilde{S}\right), \ \tilde{y} = 0, \quad -\frac{\partial \tilde{S}}{\partial \tilde{y}} = 0, \ \tilde{y} = 1. \tag{30}$$

We assume a positive velocity of the traveling front wave ($\tilde{u}>0$) that accompanies the switch of the system from one uniform steady state ($\xi \to +\infty$, $\tilde{P}=0$, $\tilde{S}=0$) to the other uniform steady state ($\xi \to -\infty$, $\tilde{P}=1$, $\tilde{S}=1$). Solution for a negative velocity can be found analogously. We set $\tilde{S} = \tilde{C}_T$ at $\xi = 0$, $\tilde{y} = 0$ and assume that the ligand and protease concentrations as well as the ligand flux are continuous functions at $\xi = 0$.

The solution is found simultaneously for both negative ($\xi \le 0$) and positive ($\xi \ge 0$) domains. In the first step, the front wave of protease activity is explicitly found

$$\tilde{P}(\xi) = 1 - \exp\left(\frac{\xi}{\tilde{u}}\right), \quad \xi \in (-\infty; 0], \tag{31}$$

$$\tilde{P}(\xi) = 0, \quad \xi \in [0; +\infty). \tag{32}$$

Equations 31 and 32 are then substituted into Eq. 30. The obtained self-adjoint eigenvalue problem can be solved by the finite Fourier transform techniques (36,51). The distribution of the dimensionless ligand concentration is found in the form of an infinite sum

$$\tilde{S}\left(\xi, \tilde{y}\right) = \sum_{n=1}^{\infty}\left[N_{2,n}\exp(\varepsilon_{1,n}\xi) + M_n \exp\left(\frac{\xi}{\tilde{u}}\right)\right] \times \psi_n\left(\tilde{y}\right) + \tilde{P}(\xi), \xi \in (-\infty; 0], \tag{33}$$

$$\tilde{S}\left(\xi, \tilde{y}\right) = \sum_{n=1}^{\infty} N_{1,n}\exp(\varepsilon_{2,n}\xi) \times \psi_n\left(\tilde{y}\right), \xi \in [0; +\infty). \tag{34}$$

Indexed constants $N_{1,n}$, $N_{2,n}$, and M_n are given by

$$M_n = D_n\left[1/\tilde{u}^2 + \left(\tau_S\tilde{u} - \mathrm{Pe}\right)\Big/\tilde{u} - \lambda_n^2/\alpha^2\right]^{-1}, \quad (35)$$

$$D_n = C_n/\lambda_n\left[1/\tilde{u}^2 + \tau_S - \mathrm{Pe}/\tilde{u}\right], \quad (36)$$

$$N_{j,n} = \frac{C_n - M_n\lambda_n + M_n\lambda_n\tilde{u}\varepsilon_{j,n}}{\tilde{u}\lambda_n(\varepsilon_{1,n} - \varepsilon_{2,n})},\ j = 1, 2. \quad (37)$$

Constants $\varepsilon_{(1,n),(2,n)}$, i.e., roots of the characteristic equation of the transformed problem, are evaluated from

$$\varepsilon_{(1,n),(2,n)} = \left[\mathrm{Pe} - \tau_S\tilde{u} \pm \sqrt{\left(\tau_S\tilde{u} - \mathrm{Pe}\right)^2 + 4\lambda_n^2/\alpha^2}\right]\Big/2. \quad (38)$$

The symbols $\psi_n(\tilde{y})$ and λ_n in Eqs. 33 and 34 denote the corresponding orthonormal eigenfunctions and eigenvalues, respectively,

$$\psi_n\left(\tilde{y}\right) = C_n\left[\cot(\lambda_n)\cos\left(\lambda_n\tilde{y}\right) + \sin\left(\lambda_n\tilde{y}\right)\right], \quad (39)$$

where

$$C_n = \sqrt{\frac{2\lambda_n}{\cot\lambda_n + \lambda_n\csc^2\lambda_n}}, \quad (40)$$

and

$$\lambda_n = \alpha\beta\cot(\lambda_n). \quad (41)$$

Roots of the transcendental Eq. 41 can be found numerically by the Newton method.

M.P. thanks S. Y. Shvartsman, Princeton University, for productive discussion on the reported problem.

The authors thank the Ministry of Education, Youth and Sports of the Czech Republic (project KONTAKT ME10036), and the Czech Science Foundation (project GA203/09/2091) for financial support.

REFERENCES

1. Heldin, C. H. 2011. Functioning of transmembrane receptors in cell signaling. Academic Press, San Diego, CA.
2. Mandell, J. W., N. C. Gocan, and S. R. Vandenberg. 2001. Mechanical trauma induces rapid astroglial activation of ERK/MAP kinase: evidence for a paracrine signal. *Glia.* 34:283–295.
3. Kim, H. G., J. Kassis, …, A. Wells. 1999. EGF receptor signaling in prostate morphogenesis and tumorigenesis. *Histol. Histopathol.* 14:1175–1182.
4. Swartz, M. A. 2003. Signaling in morphogenesis: transport cues in morphogenesis. *Curr. Opin. Biotechnol.* 14:547–550.
5. Cartwright, J. H. E., O. Piro, and I. Tuval. 2004. Fluid-dynamical basis of the embryonic development of left-right asymmetry in vertebrates. *Proc. Natl. Acad. Sci. USA.* 101:7234–7239.
6. Okada, Y., S. Takeda, …, N. Hirokawa. 2005. Mechanism of nodal flow: a conserved symmetry breaking event in left-right axis determination. *Cell.* 121:633–644.
7. Rutkowski, J. M., and M. A. Swartz. 2007. A driving force for change: interstitial flow as a morphoregulator. *Trends Cell Biol.* 17:44–50.
8. Lee, D. Y., Y. S. J. Li, …, S. Chien. 2010. Oscillatory flow-induced proliferation of osteoblast-like cells is mediated by alpha(v)beta(3) and beta(1) integrins through synergistic interactions of focal adhesion kinase and Shc with phosphatidylinositol 3-kinase and the Akt/mTOR/p70S6K pathway. *J. Biol. Chem.* 285:30–42.
9. Shi, Z. D., X. Y. Ji, …, J. M. Tarbell. 2009. Interstitial flow promotes vascular fibroblast, myofibroblast, and smooth muscle cell motility in 3-D collagen I via upregulation of MMP-1. *Am. J. Physiol. Heart Circ. Physiol.* 297:H1225–H1234.
10. Shi, Z. D., X. Y. Ji, …, J. M. Tarbell. 2010. Interstitial flow induces MMP-1 expression and vascular SMC migration in collagen I gels via an ERK1/2-dependent and c-Jun-mediated mechanism. *Am. J. Physiol. Heart Circ. Physiol.* 298:H127–H135.
11. Boardman, K. C., and M. A. Swartz. 2003. Interstitial flow as a guide for lymphangiogenesis. *Circ. Res.* 92:801–808.
12. Helm, C. L. E., M. E. Fleury, …, M. A. Swartz. 2005. Synergy between interstitial flow and VEGF directs capillary morphogenesis in vitro through a gradient amplification mechanism. *Proc. Natl. Acad. Sci. USA.* 102:15779–15784.
13. Semino, C. E., R. D. Kamm, and D. A. Lauffenburger. 2006. Autocrine EGF receptor activation mediates endothelial cell migration and vascular morphogenesis induced by VEGF under interstitial flow. *Exp. Cell Res.* 312:289–298.
14. Hernández Vera, R., E. Genové, …, C. E. Semino. 2009. Interstitial fluid flow intensity modulates endothelial sprouting in restricted Src-activated cell clusters during capillary morphogenesis. *Tissue Eng. Part A.* 15:175–185.
15. Pozrikidis, C. 2010. Numerical simulation of blood and interstitial flow through a solid tumor. *J. Math. Biol.* 60:75–94.
16. Song, J. W., and L. L. Munn. 2011. Fluid forces control endothelial sprouting. *Proc. Natl. Acad. Sci. USA.* 108:15342–15347.
17. Shieh, A. C., and M. A. Swartz. 2011. Regulation of tumor invasion by interstitial fluid flow. *Phys. Biol.* 8:015012.
18. Bobo, R. H., D. W. Laske, …, E. H. Oldfield. 1994. Convection-enhanced delivery of macromolecules in the brain. *Proc. Natl. Acad. Sci. USA.* 91:2076–2080.
19. Chen, D., D. Norris, and Y. Ventikos. 2009. The active and passive ciliary motion in the embryo node: a computational fluid dynamics model. *J. Biomech.* 42:210–216.
20. Nguyen, T. H., A. Eichmann, …, V. Fleury. 2006. Dynamics of vascular branching morphogenesis: the effect of blood and tissue flow. *Phys. Rev. E Stat. Nonlin. Soft Matter Phys.* 73:061907.
21. Fleury, M. E., K. C. Boardman, and M. A. Swartz. 2006. Autologous morphogen gradients by subtle interstitial flow and matrix interactions. *Biophys. J.* 91:113–121.
22. Luss, D., and M. Sheintuch. 2005. Spatiotemporal patterns in catalytic systems. *Catal. Today.* 105:254–274.
23. Sheintuch, M., and O. Nekhamkina. 2003. Thermal patterns in simple models of cylindrical reactors. *Chem. Eng. Sci.* 58:1441–1451.
24. Nekhamkina, O., and M. Sheintuch. 2008. Transversal moving-front patterns: criteria and simulations for two bed and cylindrical shell packed-bed reactors. *Chem. Eng. Sci.* 63:3716–3726.
25. Dixon, J. B., S. Raghunathan, and M. A. Swartz. 2009. A tissue-engineered model of the intestinal lacteal for evaluating lipid transport by lymphatics. *Biotechnol. Bioeng.* 103:1224–1235.
26. Dobens, L. L., and L. A. Raftery. 2000. Integration of epithelial patterning and morphogenesis in *Drosophila* ovarian follicle cells. *Dev. Dyn.* 218:80–93.
27. Pribyl, M., C. B. Muratov, and S. Y. Shvartsman. 2003. Long-range signal transmission in autocrine relays. *Biophys. J.* 84:883–896.

28. Muratov, C. B., F. Posta, and S. Y. Shvartsman. 2009. Autocrine signal transmission with extracellular ligand degradation. *Phys. Biol.* 6: 016006.

29. Ng, C. P., C. L. E. Helm, and M. A. Swartz. 2004. Interstitial flow differentially stimulates blood and lymphatic endothelial cell morphogenesis in vitro. *Microvasc. Res.* 68:258–264.

30. Tomei, A. A., S. Siegert, …, M. A. Swartz. 2009. Fluid flow regulates stromal cell organization and CCL21 expressions in a tissue-engineered lymph node microenvironment. *J. Immunol.* 183:4273–4283.

31. Haessler, U., Y. Kalinin, …, M. Wu. 2009. An agarose-based microfluidic platform with a gradient buffer for 3D chemotaxis studies. *Biomed. Microdevices.* 11:827–835.

32. Chang, S. F., C. A. Chang, …, J. J. Chiu. 2008. Tumor cell cycle arrest induced by shear stress: roles of integrins and Smad. *Proc. Natl. Acad. Sci. USA.* 105:3927–3932.

33. Shamloo, A., N. Ma, …, S. C. Heilshorn. 2008. Endothelial cell polarization and chemotaxis in a microfluidic device. *Lab Chip.* 8:1292–1299.

34. Park, J. Y., S. J. Yoo, …, S. H. Lee. 2009. Simultaneous generation of chemical concentration and mechanical shear stress gradients using microfluidic osmotic flow comparable to interstitial flow. *Lab Chip.* 9:2194–2202.

35. Shin, H. S., H. J. Kim, …, N. L. Jeon. 2009. Shear stress effect on transfection of neurons cultured in microfluidic devices. *J. Nanosci. Nanotechnol.* 9:7330–7335.

36. Deen, W. M. 1998. Analysis of Transport Phenomena. Oxford University Press, New York.

37. Bird, R. B., W. E. Stewart, and E. N. Lightfoot. 2002. Transport Phenomena. John Wiley & Sons, New York.

38. White, F. M. 1994. Fluid Mechanics. McGraw-Hill, New York.

39. Qiao, L., R. B. Nachbar, …, S. Y. Shvartsman. 2007. Bistability and oscillations in the Huang-Ferrell model of MAPK signaling. *PLOS Comput. Biol.* 3:1819–1826.

40. Shvartsman, S. Y., M. P. Hagan, …, D. A. Lauffenburger. 2002. Autocrine loops with positive feedback enable context-dependent cell signaling. *Am. J. Physiol. Cell Physiol.* 282:C545–C559.

41. Ferrell, Jr., J. E., and E. M. Machleder. 1998. The biochemical basis of an all-or-none cell fate switch in *Xenopus* oocytes. *Science.* 280:895–898.

42. Pribyl, M., C. B. Muratov, and S. Y. Shvartsman. 2003. Discrete models of autocrine cell communication in epithelial layers. *Biophys. J.* 84:3624–3635.

43. Shvartsman, S. Y., H. S. Wiley, …, D. A. Lauffenburger. 2001. Spatial range of autocrine signaling: modeling and computational analysis. *Biophys. J.* 81:1854–1867.

44. Doedel, E. J., and B. E. Oldeman. 2009. AUTO-07P: Continuation and bifurcation software for ordinary differential equations. Concordia University, Montreal, Canada.

45. Aris, R. 1956. On the dispersion of a solute in a fluid flowing through a tube. *Proc. R. Soc. Lond. A Math. Phys. Sci.* 235:67–77.

46. Kolev, S. D., and W. E. van der Linden. 1991. Laminar dispersion in parallel plate sections of flow systems used in analytical chemistry and chemical engineering. *Anal. Chim. Acta.* 247:51–60.

47. Grayson, W. L., M. Fröhlich, …, G. Vunjak-Novakovic. 2010. Engineering anatomically shaped human bone grafts. *Proc. Natl. Acad. Sci. USA.* 107:3299–3304.

48. Chung, S., R. Sudo, …, R. D. Kamm. 2010. Microfluidic platforms for studies of angiogenesis, cell migration, and cell-cell interactions. *Ann. Biomed. Eng.* 38:1164–1177.

49. Galie, P. A., and J. P. Stegemann. 2011. Simultaneous application of interstitial flow and cyclic mechanical strain to a three-dimensional cell-seeded hydrogel. *Tissue Eng. Part C Methods.* 17:527–536.

50. Krakstad, C., and M. Chekenya. 2010. Survival signalling and apoptosis resistance in glioblastomas: opportunities for targeted therapeutics. *Mol. Cancer.* 9:135.

51. Varma, A., and M. Morbidelli. 1997. Mathematical Methods in Chemical Engineering. Oxford University Press, New York.